molecules

MDPI

Article

Aggregation Behavior and Application Properties of Novel Glycosylamide Quaternary Ammonium Salts in Aqueous Solution

Yunkai Wang [1], Zeyu Chen [1], Erzhuang Zhang [1], Lifei Zhi [1,*], Martino Di Serio [2], Guoyong Wang [1], Yan Wang [1], Xiaoming Li [1], Xudong Liu [3] and Ying Huang [4,5]

[1] College of Chemical Engineering and Technology, Taiyuan University of Science and Technology, Taiyuan 030024, China; wyk990306@163.com (Y.W.); czy15535371231@163.com (Z.C.); aa1162791419@163.com (E.Z.); wanggy@tyust.edu.cn (G.W.); kdwyan@126.com (Y.W.); lxmlily2014@126.com (X.L.)
[2] Department of Chemical Sciences, University of Naples Federico II, 80138 Napoli, Italy; martion.diserion@gmail.com
[3] Research Institute of Livestock and Aquatic Product Inspection, Shanxi Inspection and Testing Center, Taiyuan 030006, China; 13835179079@163.com
[4] Taiyuan Hengdeyuan Animal Protection Technology Development Co., Ltd., Taiyuan 030003, China; huangying0351@163.com
[5] Shanxi Livestock and Poultry Breeding Co., Ltd., Jinzhong 031800, China
* Correspondence: lifeizhi@yeah.net or lifeizhi@tyust.edu.cn

Abstract: Amidation of lactobionic acid with N,N-dimethylaminopropyltriamine was conducted to obtain N-(3′-dimethylaminopropyl)-lactamido-3-aminopropane (DDLPD), which was quaternized with bromoalkanes of different carbon chain lengths to synthesize double-stranded lactosylamide quaternary ammonium salt N-[N′[3-(lactosylamide)]propyl-N′-alkyl] propyl-N,N-dimethyl-N-alkylammonium bromide (C_nDDLPB, n = 8, 10, 12, 14, 16). The surface activity and the adsorption and aggregation behaviors of the surfactants were investigated via equilibrium surface tension, dynamic light scattering, and cryo-electron microscopy measurements in an aqueous solution. The application properties of the products in terms of wettability, emulsification, foam properties, antistatic, salt resistance, and bacteriostatic properties were tested. C_nDDLPB exhibited a low equilibrium surface tension of 27.82 mN/m. With an increase in the carbon chain length, the critical micellar concentration of C_nDDLPBD decreased. Cryo-electron microscopy revealed that all products except C_8DDLPB formed stable monolayer, multi-layer, and multi-compartmental vesicle structures in an aqueous solution. C_{14}DDLPB has the best emulsification performance on soybean oil, with a time of 16.6 min; C_{14}DDLPB has good wetting and spreading properties on polytetrafluoroethylene (PTFE) when the length of carbon chain is from 8 to 14, and the contact angle can be lowered to 33°~40°; C_nDDLPB has low foam, which is typical of low-foaming products; C_8DDLPB and C_{10}DDLPB both show good antistatic properties. C_8DDLPB and C_{14}DDLPB have good salt resistance, and C_{12}DDLPB has the best antimicrobial property, with the inhibition rate of 99.29% and 95.28% for E. coli and Gluconococcus aureus, respectively, at a concentration of 350 ppm.

Keywords: surfactant; lactose amide; quaternary ammonium salts; surface activity; vesicle

check for updates

Citation: Wang, Y.; Chen, Z.; Zhang, E.; Zhi, L.; Di Serio, M.; Wang, G.; Wang, Y.; Li, X.; Liu, X.; Huang, Y. Aggregation Behavior and Application Properties of Novel Glycosylamide Quaternary Ammonium Salts in Aqueous Solution. *Molecules* **2024**, *29*, 2749. https://doi.org/10.3390/molecules29122749

Academic Editors: Khristo Khristov and Plamen Tchoukov

Received: 8 May 2024
Revised: 4 June 2024
Accepted: 6 June 2024
Published: 9 June 2024

Copyright: © 2024 by the authors. Licensee MDPI, Basel, Switzerland. This article is an open access article distributed under the terms and conditions of the Creative Commons Attribution (CC BY) license (https://creativecommons.org/licenses/by/4.0/).

1. Introduction

Among global environmental issues, carbon emissions have become a key issue that has received a lot of attention [1,2]. Of particular note is China's high level of carbon emissions between 2009 and 2022 [3]. To address this challenge, China made a solemn commitment at the 75th session of the United Nations General Assembly to adopt dual carbon targets, i.e., carbon peaking and carbon neutrality, as a part of its core carbon reduction

strategy. Owing to their green, environmentally friendly, and resource-saving characteristics, biobased chemicals are in alignment with the "dual-carbon" policy development; these chemicals are gradually becoming a new leading industry in the contemporary world of scientific and technological innovation and economic development. China's "13th Five-Year Plan" and "14th Five-Year Plan" also clearly reveal that focus will be placed on the development of biobased industries [4]. Biobased chemicals, which are derived from renewable resources, are bulk chemicals and fine chemicals prepared from biomass as raw materials, exhibiting several advantages such as carbon reduction and sustainability [5–7]. Biobased chemicals produce very little waste during their production process, and most of this waste can be recycled due to their green and healthy characteristics. Their easily degradable nature also provides an effective way to solve the pollution problem of petroleum-based plastics [8,9]. Sugars are typical representatives of biomass raw materials and prepared from natural renewable resources such as starch, exhibiting not only abundant sources but also cost-effectiveness [10]. The use of sugar groups as hydrophilic groups in surfactants endows them with several advantages: (1) Sugar groups endow surfactants with considerably good biodegradation performance and toxicological properties. Moreover, they are mild and non-irritating to the skin and eyes as well as easily biodegradable under anaerobic and aerobic conditions [11–13]. (2) Sugar groups contain multiple hydroxyl groups, the oleophobicity and hydrophilicity of which is greater than those of conventional polyoxyethylene ether surfactants; the oleophobicity of a sec-hydroxyl group is 4.5 times greater than that of polyethylene oxide. In oil–water systems, sugar-based surfactants exhibit better interfacial chemistry [14]. (3) Sugar groups exhibit higher resistance to hard water because they can form complexes with metal ions such as Ca^{2+} to form water-soluble complex ions. (4) Sugar groups also endow surfactants with insecticidal and herbicidal or antimicrobial activity [15–17]. Introducing sugar groups into the molecular structure of cationic surfactants may improve their irritation, toxicity, biodegradability, water solubility, compatibility, etc. [18]. Various cationic surfactants derived from sugar groups exhibit advantages, including green characteristics, natural and renewable raw materials, facile biodegradability, and multifunctionality; these surfactants are also safe and mild for human body. Therefore, these surfactants have globally attracted considerable research attention [19–21].

Herein, a double-chain lactide amide quaternary surfactant (C_nDDLPB), which combines the advantages of a sugar group, an amide bond, and a cationic surfactant, was synthesized via the amine ester reaction of lactobionic acid with an alkyl amine and then quaternized with bromoalkanes (the reaction and synthesis routes are shown in Figure 1), and the structures of the intermediates and products were characterized via Fourier transform infrared (IR) spectroscopy, nuclear magnetic resonance (NMR) spectroscopy, and mass spectrometry(MS). In addition, aggregation behavior and application properties of C_nDDLPB were also comprehensively investigated.

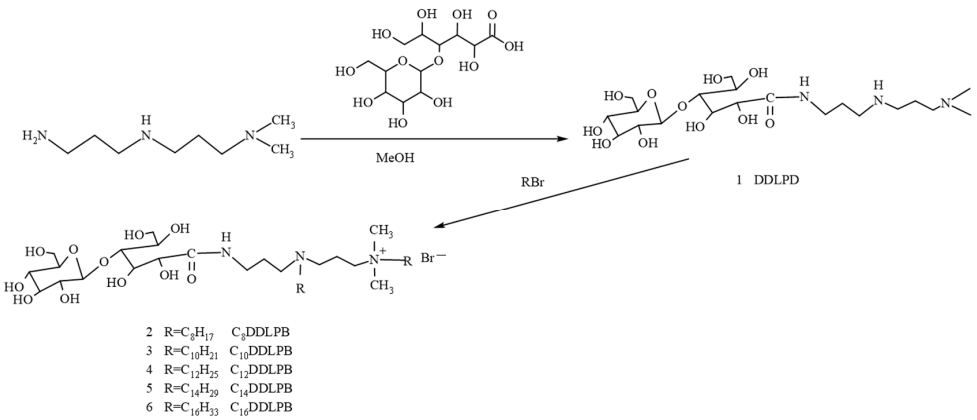


Figure 1. Synthesis roadmap of double-chain lactosamine quaternary ammonium salts (C_nDDLPB).

2. Results and Discussion

2.1. Structure Identification

The chemical structures of the raw materials, synthesized intermediates, and target compounds were characterized using FTIR, ^{1}H NMR, and ^{13}C NMR spectroscopies as well as other characterization methods. The spectra of all products are in the Supporting Information.

Figure S1a shows the FTIR spectrum of N,N-dimethyldipropylenetriamine. The peak observed at 2931 cm^{-1} corresponds to the symmetrical telescopic vibration of C–H of the methyl group, while the peak observed at 2762 cm^{-1} corresponds to the symmetrical telescopic vibration of C–H of the methylene group [22]. Figure S1b shows the FTIR spectrum of lactose. A broad and strong absorption peak observed at 3400–3200 cm^{-1} corresponds to the stretching vibration of the O–H group in lactobionic acid, the absorption peak observed at 1730 cm^{-1} corresponds to the stretching vibration of the C=O bond in lactobionic acid, and the strong peak observed at 1030 cm^{-1} corresponds to the C–O bond stretching vibration.

In the spectrum of DDLPD in Figure S1c, absorption peaks corresponding to the O–H group in lactobionic acid and C–H of N, N-dimethyldipropenyltriamine are observed; the two strong characteristic absorption peaks observed at 1650 and 1540 cm^{-1} correspond to the telescopic vibration of the C=O bond in amide groups and the bending vibration of N–H, respectively, indicating that amide bonds are generated.

2.2. Electrospray Mass Spectrometry (EMS)

The synthesized glycosylamide quaternary ammonium salt was analyzed via ESI-MS, and its composition was analyzed and identified according to its molecular weight: the relative molecular mass of the expected product C_{12}DDLPB is 916. Figure S16 shows the ESI-MS spectrum of the target product C_{12}DDLPB. The quaternary ammonium surfactant C_{12}DDLPB exhibits an $(M–H)^{+}$ quasimolecular ion peak at 915.35 (m/z). The quasimolecular ion is relatively stable after losing one electron; Br^{-} is bombarded using the positive-ion mode, and a strong $[M–Br]^{+}$ fragmentation peak is observed at m/z 836.86. The fragmentation peak of [M-Br- OH-OH]$^{+}$ is observed at m/z 746.88, the fragmentation peak of [M-Br-CH_3O-$C_2H_5O_2$-O-O]$^{+}$ is observed at m/z 612.55, and the fragmentation peak of [M-Br-CH_3O-$C_2H_5O_2$-OH-OH -H-H]$^{+}$ is observed at m/z 608.85. The m/z values of the molecular ion peaks of C_8DDLPB, C_{10}DDLPB, C_{14}DDLPB, and C_{16}DDLPB are 803.49, 862.51, 974.38, and 1029.45, respectively, which are consistent with the expected molecular masses of the products (Supplementary Material Figures S14–S18) [23].

The combined FTIR spectroscopy, ^{1}H NMR spectroscopy, ^{13}CNMR spectroscopy, and ESI-MS results reveal that the double-stranded lactose amide quaternary surfactants are successfully synthesized.

2.3. Surface Tension

The surface tension of C_nDDLPB was determined using the hanging drop method at 25 °C ± 0.1 °C. The surfactant solution was prepared from RO water; the surface tension of RO water was 72 ± 0.3 mN/m. The surface tension versus concentration curve reveals an inflection point in the concentration, corresponding to the critical micellar concentration (CMC). Before the turning point is reached (Figure 2), a linear relationship between the increase in the surfactant concentration and the decrease in surface tension is observed, indicating that the surfactant molecules begin to arrange closely at the interface. After reaching the CMC, the surface tension remains constant.

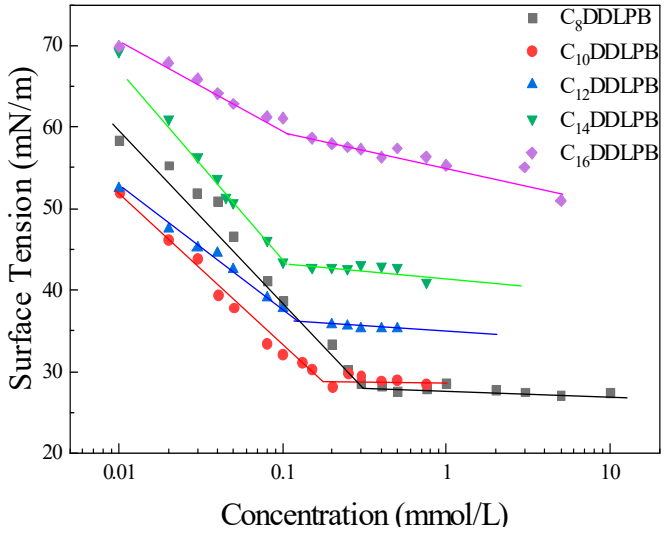


Figure 2. Surface tension of C_nDDLPB in an aqueous solution as a function of concentration.

According to Equations (1)–(3) [24,25], the amount of adsorption at saturation at the gas/liquid interface (Γ_{max}), cross-sectional area per molecule A_{min}, and surface activity efficiency pC_{20} can be estimated:

$$\Gamma_{max} = -\frac{1}{2.303nRT}\left(\frac{\partial\gamma}{\partial lgc}\right)_T \quad (1)$$

$$A_{min} = \frac{10^{16}}{N_A\Gamma_{max}} \quad (2)$$

$$pC_{20} = -logC_{20} \quad (3)$$

where γ represents the surface tension, mN/m; T represents the absolute temperature, K; and R represents the gas constant, 8.314 J/(mol·K). Moreover, the value of n for an ionic surfactant type 1-1 is considered to be 2, N_A represents the Avogadro constant, and C_{20} represents the concentration of the surfactant required to reduce the surface tension of water by 20 mN/m.

CMC/C_{20} indicates the difficulty and simplicity of the surfactant adsorption and micellization process. The higher CMC/C_{20}, the easier the tendency for the surfactant to adsorb on the interface than that to form a micelle.

The CMC values of the five double-chain lactose amide quaternary ammonium salts (C_nDDLPB) decrease in the order of C_8DDLPB > C_{10}DDLPB > C_{12}DDLPB > C_{14}DDLPB > C_{16}DDLPB (Figure 3). Their CMC values decrease linearly with the growth of the hydrophobic carbon chain [26]. This result is attributed to the fact that, when two carbon chains of the surfactant molecule become longer, the space occupied by the molecules arranged at the interface is saturated more rapidly. The larger the space occupied by the two carbon chains of the surfactant molecules, the faster the molecules arranged at the interface reach saturation; at the same time, the longer the carbon chains, the hydrophobicity of the hydrocarbon bonds is gradually enhanced, indicating that the separation formed between the hydrophilic head groups under the action of electrostatic repulsive force is hindered, rendering a significant promotion effect on the development of aggregates in the surfactants. The shorter the carbon chain, the lower the surface tension. The surface tension of the C_8DDLPB aqueous solution can be reduced to 27.82 mN/m. The inflection point of CMC on the curve of the change in the surface tension with the C_{16}DDLPB concentration is not extremely clear, which may be attributed to the fact that the two hydrophobic carbon chains are extremely long and lead to poor solubility and a low surface activity.

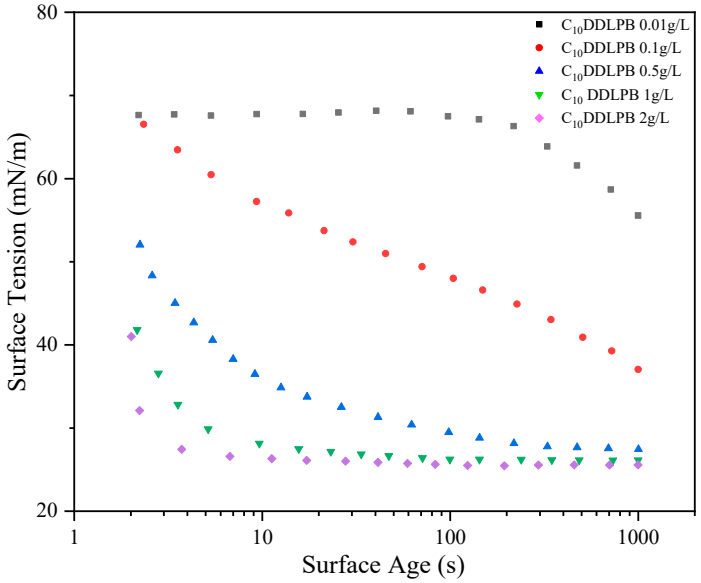


Figure 3. Dynamic surface tensions vs. surface age for 0.01 g/L–2 g/L C_nDDDLPB.

With an increase in the length of the carbon chain, Γ_{max} decreases (Table 1). When the carbon chain becomes longer, the obstruction of the molecules to occupy a position in space increases. The possibility of the dense arrangement of molecules within the unit surface decreases, and the cross-sectional area Amin per molecule increases. The pC_{20} value of C_{10}DDLPB is the highest, indicative of the higher adsorption efficiency at the interface.

Table 1. Surface adsorption and aggregation parameters of C_nDDLPB in aqueous solution.

Surfactant	CMC (mmol/L)	Γ_{cmc} (mN/m)	pC_{20}	CMC/C_{20}	Γ_{max} (mol·cm^{-2})	A_{min} (Å^2)	ΔG^0_{mic} (KJ·mol^{-1})	ΔG^0_{ads} (KJ·mol^{-1})
C_8DDLPB	0.333	27.82	4.585	12.808	1.890×10^{-10}	87.857	−59.96	−64.85
C_{10}DDLPB	0.136	30.27	5.046	15.111	1.675×10^{-10}	99.15	−62.75	−67.05
C_{12}DDLPB	0.12	36.11	4.971	11.215	1.275×10^{-10}	130.266	−64.66	−67.74
C_{14}DDLPB	0.106	43.1	4.343	2.335	1.198×10^{-10}	138.603	−65.33	−67.12
C_{16}DDLPB	0.103	59.09	2.356	0.023	8.365×10^{-11}	198.509	−65.28	−66.81

2.4. Dynamic Surface Tension

Dynamic surface tension can be used to study the adsorption–diffusion kinetics of surfactants at the air–water interface. In this study, the dynamic surface tension changes in C_{10}DDLPB were measured in the concentration range of 0.01 g/L–2 g/L by the suspended droplet method, and the dynamic surface tension of C_nDDLPB with five different carbon chain lengths at a concentration of 1 g/L (25 °C) was measured in detail.

Figure 3 demonstrates the dynamic surface tension curves of C_{10}DDLPB at different concentrations, from which it can be seen that the surface activity increases with increasing concentration, and the higher the concentration, the faster the adsorption rate.

Figure 4 demonstrates the surface tension versus surface age plots of C_nDDLPB with different carbon chain lengths at 1 g/L concentration. With the increase in surface age, the surface tension of each surfactant gradually decreased and finally reached a stable value. This indicates that the C_nDDLPB molecules undergo the process of diffusion–adsorption, reaching a steady state at the liquid surface. The ability to reduce the surface tension has a tendency to increase with the decrease in carbon chain length, which may be related to the fact that the shorter carbon chain molecules are easier to be arranged and form a compact structure at the interface. However, it is noteworthy that the adsorption rates of the surfactants increased with decreasing carbon chain length, except for C_8DDLPB, for which this anomaly may be attributed to the shorter hydrophobic chain.

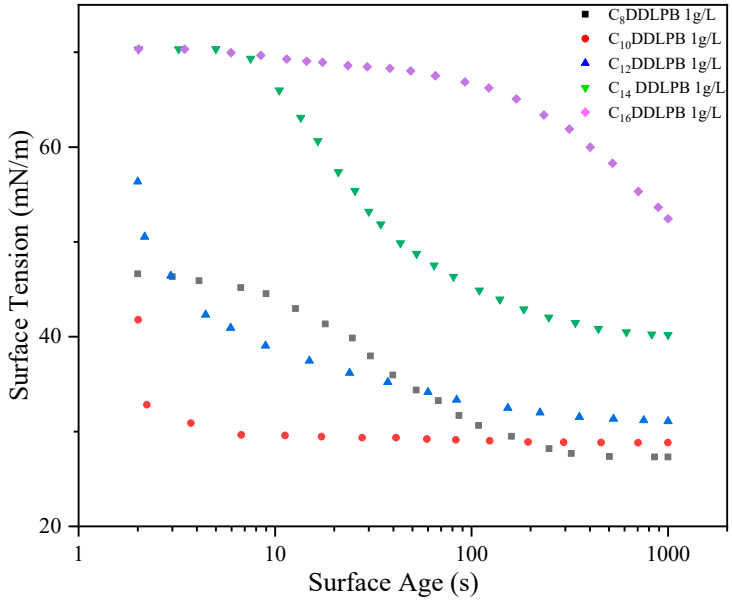


Figure 4. Dynamic surface tensions vs. surface age for 1 g/L C_nDDDLPB.

2.5. Aggregation Behavior in Aqueous Solutions

The aggregation behavior of C_nDDLPB at a concentration of 5 g/L in aqueous solution was observed using cryo-transmission electron microscopy (Cryo-TEM) at a magnification of 92,000 times, as shown in Figure 5. Except for C_8DDLPB, which forms ordinary micelles with a diameter of approximately 20 nm in an aqueous solution, the other samples form single-layered, multi-layered, or multi-compartmental vesicle structures, with vesicle diameters ranging from approximately 100 to 400 nm. Among them, C_{10}DDLPB and C_{12}DDLPB formed multi-compartmental vesicles, and C_{14}DDLPB and C_{16}DDLPB formed single-layer vesicle structures. Figure 5b,c and Supporting Information Figure S19b,c show the cryogenic transmission electron microscopy images of C_{10}DDLPB samples kept for 1 month and 24 h, respectively. The magnification of the cryo-electron microscope in the Supporting Information is 45,000×. With an increase in the time of placing the samples, more vesicles are formed, indicating that the vesicle-forming system is more stable with an increase in the sample storage time and that more vesicles are aggregated to form a multi-compartmental vesicle structure. The results reveal that the vesicle-forming system is more stable with an increase in the sample storage time.

The appearance of the prepared solutions also reveals that C_8DDLPB is a translucent light gray solution and that C_{10}DDLPB-C_{16}DDLPB is a light blue solution. During vesicle formation, surfactant molecules aggregate at the water–oil interface and form a closed structure with hydrophobic chains inside and hydrophilic chains outside. The length of the hydrophobic chains is critical to the stability of the vesicles. Surfactant molecular structures with two hydrocarbon chains and large head groups are prone to spontaneous vesicle formation [27–29]. The molecular structure of the surfactant synthesized herein (C_nDDLPB) is in agreement with such features. However, in case of a short-carbon chain, sufficient hydrophobic forces cannot be provided to maintain the stability of vesicles, resulting in the facile rupture of vesicles. In addition, surfactant molecules with a short-carbon chains exhibit a high degree of expansion in an aqueous solution, indicating that the formation of tight aggregation structures by these short-carbon chains is difficult and that water molecules cannot be wrapped effectively to form complete vesicle structures.

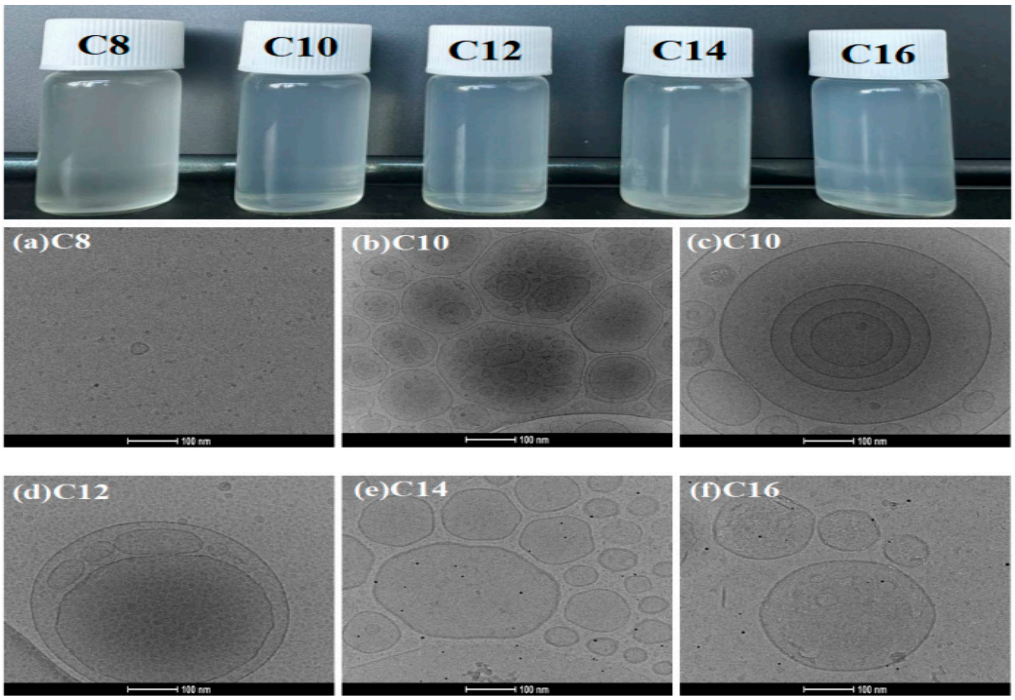


Figure 5. Aggregation behavior of C_nDDLPB under cryo-electron microscopy.

The mechanism of C_nDDLPB solution vesicle formation is shown in Figure 6: (1) First, C_nDDLPB surfactant molecules are dissolved in water, and the hydrophilic head interacts with water molecules and is surrounded by them, which are dispersed in solution as monomers. (2) Formation of micelles: at the water/oil interface or water/air interface, the hydrophobic tails of the surfactant molecules interact with the oil or air phase, leading to the adsorption of the molecules on the interface. Formation of a stable interface: when the solution concentration reaches the CMC, the active molecules form monolayer micelles [30]. (3) Formation of flexible bilayers: With an increase in the concentration, the micelles begin to disperse and reorganize into flexible bilayer structures. With an increase in the size of the molecular films, they begin to inwardly bend spontaneously to form curved structures to reduce edge energy; this closure can be facilitated by hydrophobic forces between the hydrophobic tails [31,32]. (4) Unstable vesicles: when the bilayer is completely closed, small unstable vesicles are formed [33]. (5) Formation of stable large vesicles: Over time, multiple small vesicles merge with each other to form a stable large vesicle [34,35]. The ultimate stability of a vesicle depends on the balance between hydrophobic effects and surface tension. The stronger the interaction force of the hydrophobic tail, the higher the stability of the vesicle. At the same time, the film formed by surfactant molecules at the interface can also reduce the surface energy of the system and make the vesicle structure more stable. C_{10}DDLPB and C_{12}DDLPB exhibit the best balance of the hydrophobic effect and surface tension, which are more likely to aggregate on the membrane surface and induce the neighboring layers to come closer together, leading to the gradual stacking of the membrane layers to form multi-layer and multi-compartmental structures.

Most cationic surfactants cannot spontaneously form vesicles. Therefore, C_nDDLPB with a long-carbon chain demonstrates good application prospects in slow-release drug carriers, template agents, biofilm mimicry, microreactors, and the cosmetic and food industries.

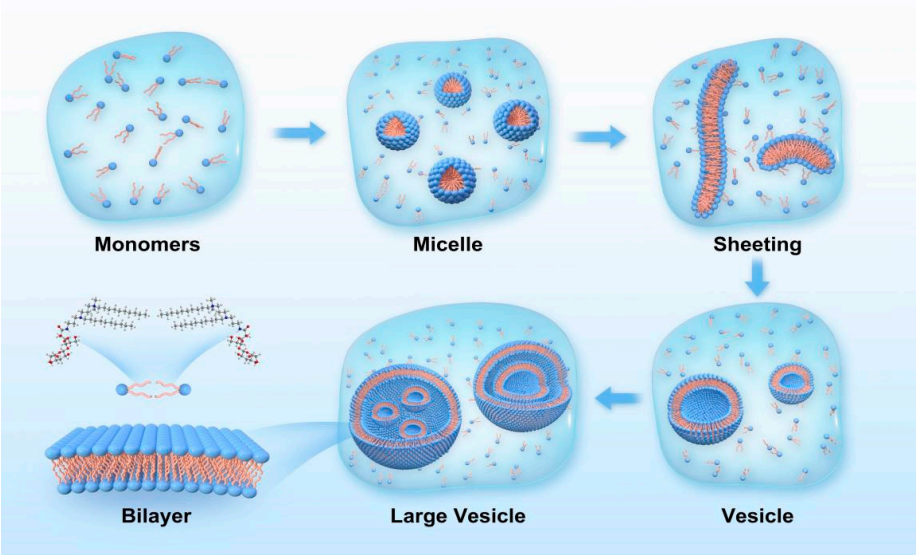


Figure 6. Schematic diagram of the vesicle formation of C_nDDLPB.

Figure 7 shows the particle size distribution of the 5 g/L C_nDDLPB sample. C_nDDLPB exhibits a single-peak particle distribution, and the overall particle sizes range from 20 nm to 1000 nm. The particle sizes of C_{16}DDLPB and C_{10}DDLPB exhibit a narrower distribution between 50 nm and 400 nm (Figure 7a,d), indicating that the diameters of the formed aggregates are mainly concentrated in this range. The particle size distribution of the C_{14}DDLPB solution becomes narrower between 50 nm and 380 nm (Figure 7b), indicating that the distribution is more concentrated. The particle size distribution shown in Figure 7c is between 50 nm and 700 nm, which is a wider particle size distribution than those of other samples, indicating that the size of the formed aggregates is larger. As shown in Figure 7e, the particle size of this solution is mainly distributed between 20 nm and 80 nm, indicating that larger aggregates are not formed, which is consistent with the TEM results, and the system only forms micelles without vesicle formation.

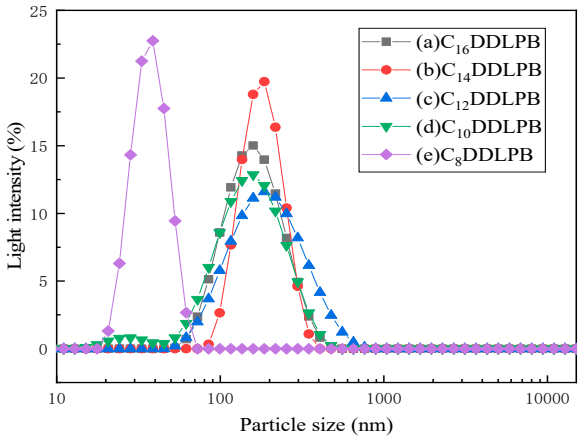


Figure 7. Particle size distributions of (**a**) C_{16}DDLPB, (**b**) C_{14}DDLPB, (**c**) C_{12}DDLPB, (**d**) C_{10}DDLPB, and (**e**) C_8DDLPB.

2.6. Wetting Ability

The changes in contact angles between different concentrations of C_nDDLPB and PTFE over time are illustrated in Figure 8. It is evident from the graph that the contact angles of C_nDDLPB on the surface of PTFE decrease with the increasing concentration.

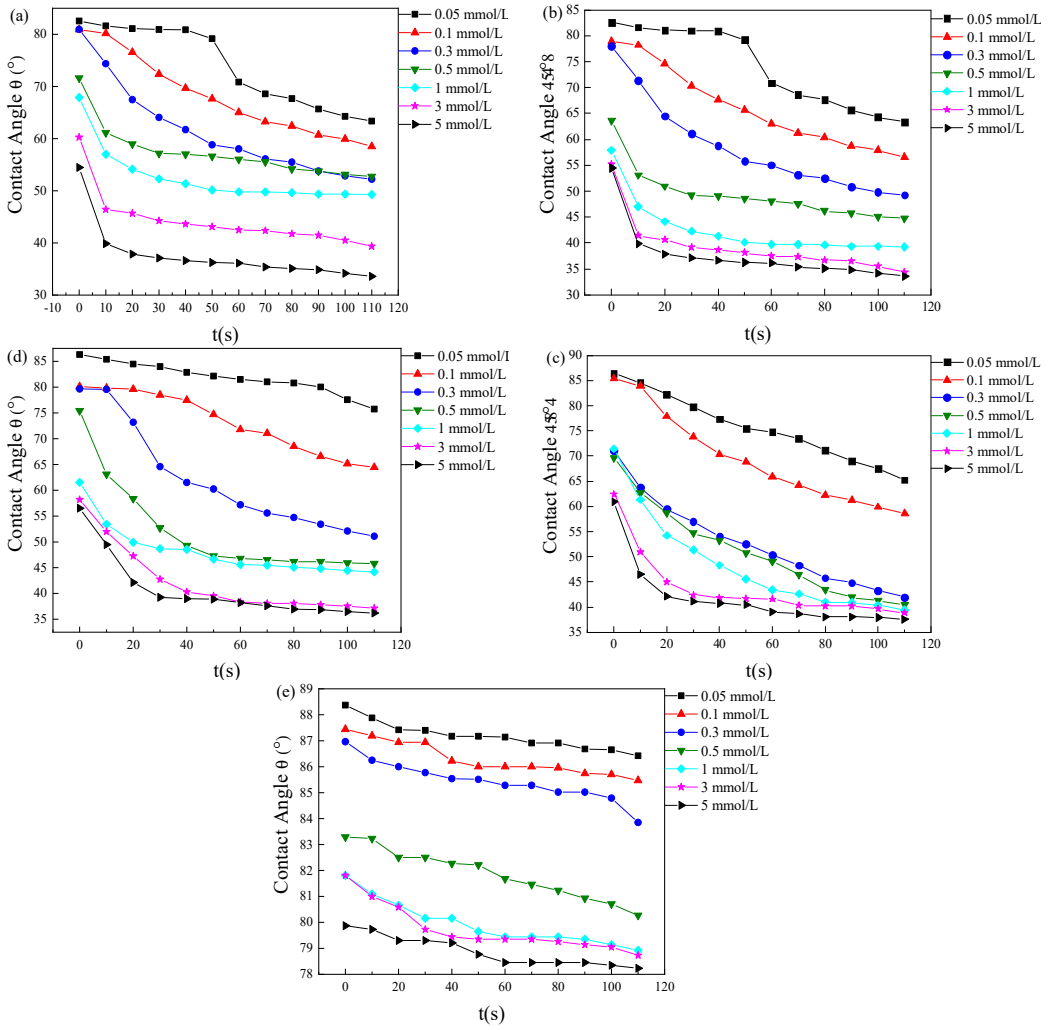


Figure 8. The effect of surfactant concentration on the contact angle of PTFE surface: (**a**) C_8DDLPB, (**b**) C10DDLPB, (**c**) C12DDLPB, (**d**) C14DDLPB, and (**e**) C16DDLPB.

In this study, C_8DDLPB, C_{10}DDLPB, C_{12}DDLPB, and C_{14}DDLPB have demonstrated favorable wetting properties on the PTFE surface, with contact angles reducing to 33°~38°. Particularly, C_8DDLPB and C_{10}DDLPB exhibit the ability to reduce the surface tension of water to 27.82 and 30.27 mN/m, respectively. Conversely, C_{16}DDLPB shows the least wetting ability, with a contact angle only decreasing to 78° within 110 s. Its equilibrium surface tension value is measured at 59 mN/m. These findings suggest that the wetting effect of C_nDDLPB on the PTFE surface is closely associated with its capability to lower the surface tension of water. Moreover, the impact of hydrophobic chain length in the hydrophobic group is notable [36,37].

2.7. Emulsifying Ability

The emulsification capacity test results for soybean oil are shown in Figure 9. As the carbon chain length increases, the emulsification capacity initially increases and then decreases. Specifically, C_{14}DDLPB exhibits the best emulsification performance with an emulsification time of 16.6 min, while the emulsification effect is poorest with a carbon chain length of eight. Furthermore, when the hydrophobic chain length becomes too long, as in the case of C_{16}DDLPB, the emulsification ability also weakens. This trend parallels that observed for the single-chain glucose acylamide quaternary ammonium salt C_nDGMAPB synthesized by our research group [38]. The hydrophobic chain length of C_nDDLPB significantly influences the emulsification capacity of soybean oil. Poor emulsification

performance is observed with hydrophobic chain lengths of 8 and 16, whereas a moderate hydrophobic chain length demonstrates good emulsification.

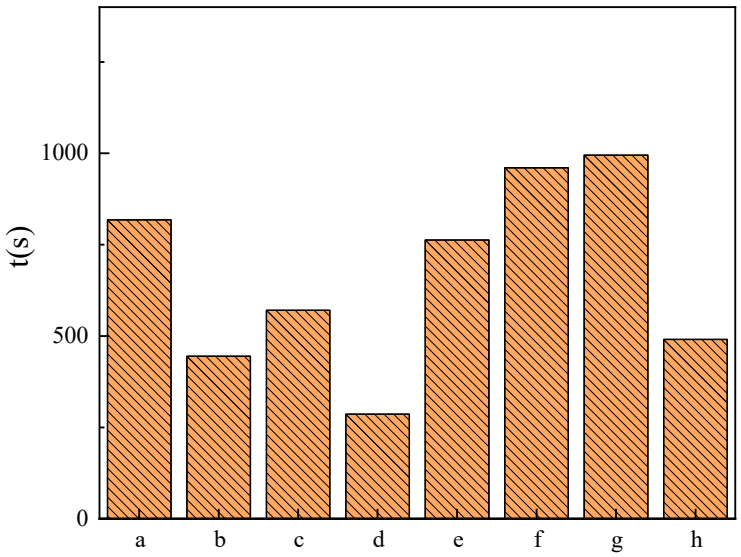


Figure 9. Emulsification time of soybean oil by surfactants: (**a**) 1227, (**b**) 1231, (**c**) HACC, (**d**) C_8DDLPB, (**e**) C_{10}DDLPB, (**f**) C_{12}DDLPB, (**g**) C_{14}DDLPB, and (**h**) C_{16}DDLPB.

2.8. Foam Properties

The foam performance of C_nDDLPB surfactants in deionized water was evaluated using the Ross–Miles method, and the results are shown in Figure 10. From the graph, it is evident that C_{12}DDLPB surfactant exhibits superior foamability, with a foam height reaching 67 mm. After 30 s, the foam height decreases by only 1 mm, and there is no further change in foam height over the subsequent 5 min, indicating excellent foam stability. However, compared to common anionic surfactants (foam height of >100 mm), it belongs to the category of low-foaming surfactants. C_8DDLPB, C_{10}DDLPB, and C_{14}DDLPB initially exhibit similar foam heights of 25 mm, 25 mm, and 22 mm, respectively, indicating relatively poor foamability. On the other hand, the foam generated by C_8DDLPB and C_{16}DDLPB dissipates rapidly, classifying them as low-foaming surfactants overall. These surfactants hold promise for applications in low-foam detergents and related products.

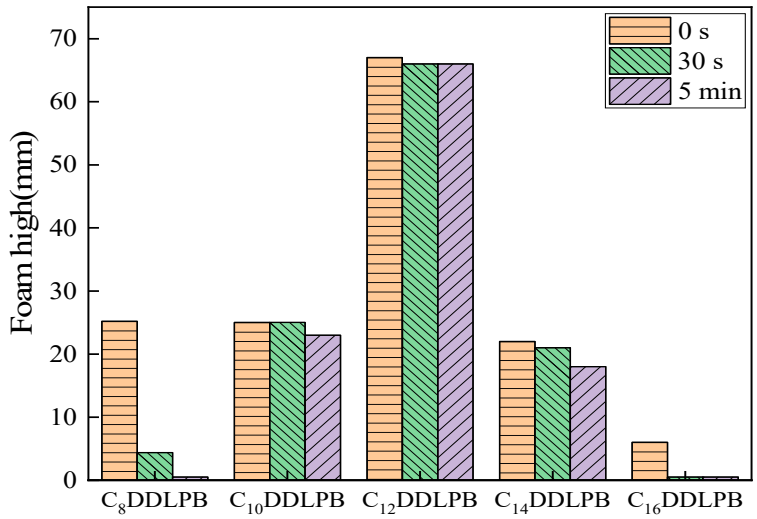


Figure 10. Graph of the foam properties of C_nDDLPB surfactants.

2.9. Antistatic Performance

The surface resistivity of polyester fabric before and after treatment was measured using a high-resistance meter, with the effectiveness of the surfactant's antistatic properties evaluated based on the magnitude of the decrease in surface resistivity logarithm values ($\triangle lg\rho_s$). A higher $\triangle lg\rho_s$ value indicates better antistatic performance. A series of synthesized lactose-based quaternary ammonium salt surfactants and commercially available antistatic agent, dihydroxyethyl stearylamine nitrate (SN), were tested, and the experimental results are presented in Table 2: at a concentration of 0.35 g/L, SN > C_8DDLPB > C_{10}DDLPB > C_{12}DDLPB > C_{14}DDLPB > C_{16}DDLPB, with C_8DDLPB exhibiting the largest $\triangle lg\rho_s$ among the C_nDDLPB surfactants, thereby indicating the best antistatic effect. The antistatic effects of C_8DDLPB and C_{10}DDLPB are approaching those of SN. Additionally, there is a trend of decreasing antistatic performance with increasing carbon chain length in C_nDDLPB.

Table 2. Antistatic properties of C_nDDLPB surfactant.

Sample Name	Concentration (g/L)	R_s/Ω	Lg (R_s/Ω)	$\Delta lg\rho_s$
Blank Control	0.35	2.70×10^{-13}	13.43	0
C_8DDLPB	0.35	2.52×10^{-10}	10.32	3.115
C_{10}DDLPB	0.35	2.29×10^{-10}	10.36	3.075
C_{12}DDLPB	0.35	4.93×10^{-12}	12.68	0.75
C_{14}DDLPB	0.35	1.99×10^{-13}	13.2	0.235
C_{16}DDLPB	0.35	2.63×10^{-13}	13.42	0.01
SN	0.35	3.41×10^{-10}	10.3	3.13

From Table 2, it can be observed that the maximum adsorption (Γ_{max}) of C_nDDLPB decreases with the increase in carbon chain length. Among the synthesized surfactants, C_8DDLPB and C_{10}DDLPB exhibit the highest Γ_{max} values, which are 1.890×10^{-10} mol·cm^{-2} and 1.675×10^{-10} mol·cm^{-2}, respectively. These results suggest that their antistatic effects may be related to their adsorption on the fabric surface.

2.10. Salt-Resistant Performance

This study investigated the salt resistance of DDAC and synthesized C_nDDLPB surfactants at different concentrations in various salt environments, as shown in Tables 3–5. When the concentration of sodium chloride added was 50 g/L, C_8DDLPB and C_{14}DDLPB exhibited transmittance rates of 94.19% and 99.08%, respectively, with excellent transmittance and no precipitation, indicating good salt resistance. In the presence of 35 g/L sodium chloride in the C_{12}DDLPB solution, the transmittance was 93.76%, demonstrating some degree of salt resistance.

Table 3. Permeability of surfactant solutions with NaCl concentration.

Concentration (g/L)	DDAC	C_8DDLPB	C_{10}DDLPB	C_{12}DDLPB	C_{14}DDLPB	C_{16}DDLPB
0	100%	100%	100%	100%	100%	100%
10	precipitates	96.83%	precipitates	100%	100%	90.16%
20	precipitates	96.38%	precipitates	100%	100%	69.98%
25	precipitates	95.72%	precipitates	98.86%	100%	precipitates
30	precipitates	95.72%	precipitates	98.17%	100%	precipitates
35	precipitates	95.06%	precipitates	93.76%	99.08%	precipitates
40	precipitates	95.06%	precipitates	64.57%	99.08%	precipitates
45	precipitates	94.62%	precipitates	precipitates	99.08%	precipitates
50	precipitates	94.19%	precipitates	precipitates	99.08%	precipitates

Table 4. Permeability of surfactant solutions with $CaCl_2$ concentration.

Concentration (g/L)	DDAC	C_8DDLPB	C_{10}DDLPB	C_{12}DDLPB	C_{14}DDLPB	C_{16}DDLPB
0	100%	100%	100%	100%	100%	100%
10	precipitates	96.83%	precipitates	100%	100%	90.16%
20	precipitates	96.38%	precipitates	100%	100%	69.98%
25	precipitates	95.72%	precipitates	98.86%	100%	precipitates
30	precipitates	95.72%	precipitates	98.17%	100%	precipitates
35	precipitates	95.06%	precipitates	93.76%	99.08%	precipitates
40	precipitates	95.06%	precipitates	64.57%	99.08%	precipitates
45	precipitates	94.62%	precipitates	precipitates	99.08%	precipitates
50	precipitates	94.19%	precipitates	precipitates	99.08%	precipitates

Table 5. Permeability of surfactant solutions with $MgSO_4$ concentration.

Concentration (g/L)	DDAC	C_8DDLPB	C_{10}DDLPB	C_{12}DDLPB	C_{14}DDLPB	C_{16}DDLPB
0	100%	100.00%	100.00%	100.00%	100.00%	100.00%
10	99.77%	99.54%	precipitates	precipitates	85.70%	precipitates
20	67.92%	99.54%	precipitates	precipitates	86.30%	precipitates
25	precipitates	99.54%	precipitates	precipitates	86.30%	precipitates
30	precipitates	99.54%	precipitates	precipitates	86.50%	precipitates
35	precipitates	99.54%	precipitates	precipitates	87.30%	precipitates
40	precipitates	99.54%	precipitates	precipitates	84.53%	precipitates
45	precipitates	99.54%	precipitates	precipitates	87.90%	precipitates
50	precipitates	99.54%	precipitates	precipitates	86.90%	precipitates

At a concentration of 50 g/L magnesium sulfate, C_8DDLPB and C_{14}DDLPB maintained transmittance rates of 99.54% and 86.90%, respectively, indicating strong salt resistance. In the presence of NaCl, $CaCl_2$, and $MgSO_4$, C_8DDLPB consistently exhibited excellent salt resistance.

In comparison with DDAC, the series of C_nDDLPB synthesized in this study have lactose-based hydrophilic groups containing numerous hydroxyl groups with strong negative polarity. Compared to micelles, these groups can readily attract more metal cations, resulting in a significant reduction in the concentration of unbound counterions in the solution, thereby hindering the formation of precipitates to some extent.

2.11. Antibacterial Performance

In this study, Gram-positive bacteria (*Staphylococcus aureus*) and Gram-negative bacteria (*Escherichia coli*) were used as samples to assess the antibacterial efficacy of C_{12}DDLPB and C_{14}DDLPB. Each group selected an appropriate dilution gradient for antibacterial rate calculation, utilizing the following formula:

$$\text{Antibacterial Rate}(\%) = \frac{\text{C - E}}{\text{C}} \times 100\% \quad (4)$$

where C denotes the average bacterial count of the control sample, and E denotes the average bacterial count of the experimental sample.

Quaternary ammonium salt surfactants carry a positive charge in water, allowing them to interact with negatively charged microbial surfaces, leading to adsorption and the formation of small aggregates that adhere to the cell wall. This process inhibits microbial growth. Additionally, the hydrophobic groups of these surfactants interact with the hydrophilic groups of microbial cells, altering the permeability of the cell membrane. This results in membrane damage and leakage of intracellular substances. Furthermore, the abundance of positive charges can coagulate and denature proteins within microbial cells, affecting cell metabolism and achieving disinfection and antibacterial effects [39].

From Tables 6 and 7, it can be observed that at a concentration of 350 ppm, C_{12}DDLPB exhibits excellent antibacterial performance against *Escherichia coli* and *Staphylococcus aureus*,

with antibacterial rates reaching 99.29% and 95.28%, respectively. Conversely, C_{14}DDLPB demonstrates poorer antibacterial efficacy, with antibacterial rates against *Escherichia coli* and *Staphylococcus aureus* at 73.20% and 76.91%, respectively. The antibacterial effect is more pronounced when the hydrophobic chain length is 12, which aligns with the previous literature [40]. Therefore, C_{12}DDLPB holds promise as a novel disinfectant product for potential applications.

Table 6. Inhibition of *Escherichia coli* by C_{12}DDLPB and C_{14}DDLPB.

Sample Name	Sample Number	Dilution Factor	CFU Prorata	Average Value	Antibacterial Rate
Control Group	*Escherichia coli*1	1.00×10^8	2.15×10^{10}	2.26×10^{10}	0
	*Escherichia coli*2	1.00×10^8	2.43×10^{10}		
	*Escherichia coli*3	1.00×10^8	2.20×10^{10}		
C_{12}DDLPB	*Escherichia coli* C12-1	1.00×10^6	1.47×10^8	1.60×10^8	99.29%
	Escherichia coli C12-2	1.00×10^6	2.01×10^8		
	Escherichia coli C12-3	1.00×10^6	1.31×10^8		
C_{14}DDLPB	*Escherichia coli* C14-1	1.00×10^7	4.89×10^9	6.06×10^9	73.20%
	Escherichia coli C14-2	1.00×10^7	6.86×10^9		
	Escherichia coli C14-3	1.00×10^7	6.42×10^9		

Table 7. Inhibition of *Gluconococcus aureus* by C_{12}DDLPB and C_{14}DDLPB.

Sample Name	Sample Number	Dilution Factor	CFU Prorata	Average Value	Antibacterial Rate
Control Group	*Staphylococcus aureus*1	1.00×10^7	3.07×10^9	3.06×10^9	0
	*Staphylococcus aureus*2	1.00×10^7	3.01×10^9		
	*Staphylococcus aureus*3	1.00×10^7	3.10×10^9		
C_{12}DDLPB	*Staphylococcus aureus* C12-1	1.00×10^6	1.41×10^8	1.44×10^8	95.28%
	Staphylococcus aureus C12-2	1.00×10^6	1.37×10^8		
	Staphylococcus aureus C12-3	1.00×10^6	1.55×10^8		
C_{14}DDLPB	*Staphylococcus aureus* C14-1	1.00×10^7	5.40×10^8	7.07×10^8	76.91%
	Staphylococcus aureus C14-2	1.00×10^7	7.50×10^8		
	Staphylococcus aureus C14-3	1.00×10^7	8.30×10^8		

3. Experimental

3.1. Materials and Instruments

Lactobionic acid (99%) was purchased from Aldrich, and chemically pure octyl bromide, decyl bromide, dodecyl bromide, tetradecyl bromide, and hexadecyl bromide were purchased from Shanghai Bohua Biochemical Reagent Co. Ltd., Shanghai, China, and N,N-dimethyl dipropylenetriamine (99.15%) was purchased from Guangdong Swell River Chemical Reagent Co. Ltd., Wengjiang, China. Deuterated dimethyl sulfoxide [DMSO] (99.9%) was purchased from Shanghai McLean Biochemical Technology Co., Shanghai, China. Didecyldimethylammonium chloride [DDAC] (95%) was purchased from Shanghai McLean Biochemical Science and Technology Co., Shanghai, China. Dodecyldimethylbenzylammonium chloride [1227] (99%) and dodecyltrimethylammonium chloride [1231] (99%) were purchased from Shanghai McLean Biochemical Science and Technology Co., Shanghai, China.

FT-IR spectrometer, model VERTEX 70 (Bruker, Saarbrücken, Germany); nuclear magnetic resonance (NMR) instrument, model AVANCE III (Bruker, Germany); electrospray ionization mass spectrometer, model Q Exactive (Thermofisher, Waltham, MA, USA); vacuum drying oven, model DZF-0B (China Yuejin Medical Equipment Co., Ltd., Shanghai, China); automatic surface tension meter, model KRÜSS-Tensíío (KRÜSS, Germany); drop shape analyzer, model DSA25B (KRÜSS, Hamburg, Germany); cryogenic transmission

electron microscopy, model Talos F200C (Thermo Fisher, Waltham, MA, USA); and dynamic light scattering instrument, model JEM-1011EX (China Baxter Instruments Co., Ltd., Dandong, China), were utilized.

3.2. Synthesis of the Intermediate N-(3′-dimethylaminopropyl)-lactamido-3-aminop-ropane (DDLPD)

Lactobionic acid (0.1 mol) and N,N-dimethyldipropylenetriamine (0.12 mol) were added to 200 mL of methanol, and the reaction was conducted under reflux conditions for 2 h. After completion of the reaction, the heating was stopped, and the reaction was allowed to cool. The solvent was evaporated using a rotary evaporator, and the resulting product was washed thrice with ether to remove the residual N,N-dimethyldipropylenetriamine, followed by drying under vacuum until a constant weight was obtained, affording the intermediate DDLPD.

3.3. Synthesis of N-[N′[3-(lactosyl amide)]propyl-N′-alkyl]propyl-N,N-dimethyl-N-alkylammonium Bromide (C_nDDLPB)

First, DDLPD (0.05 mol), bromoalkane (0.15 mol), and 200 mL of anhydrous methanol were added in a 250 mL three-neck round-bottom flask equipped with a thermometer and a spherical condenser tube. Second, the reaction was performed under reflux conditions for 10 h. After completion of the reaction, the heating was stopped, and the reaction was allowed to cool. The solvent was evaporated using a rotary evaporator, and the product was washed thrice with ether and dried under vacuum until a constant weight was obtained, affording the product C_nDDLPB.

3.4. Characterization of C_nDDLPB

The samples to be tested were tested using a VERTEX 70 Fourier transform infrared (FTIR) spectral analyzer, and the samples to be tested were pressed with KBr, which was mixed homogeneously with an appropriate amount of the samples to be tested. The raw materials N,N-dimethyldipropylenetriamine, lactobionic acid, DDLPD, and C_nDDLPB were scanned in the wavelength range of 500–4000 cm^{-1}, and the structure of the products was characterized by observing the characteristic peaks of the IR spectra generated after scanning.

The synthesized products were subjected to ^{1}H-NMR and ^{13}C-NMR measurements (internal standard was tetramethylsilane (TMS), and solvent was deuterated dimethylsulfoxide (DMSO)) using an AVANCE III NMR spectrometer, and the molecular structure of the synthesized compounds was analyzed by NMR spectroscopy.

The synthesized compounds were detected using Q Exactive electrospray ionization mass spectrometer and identified and analyzed by ESI-MS spectra.

3.5. Surface Tension

The surface tension of C_nDDLPB was determined using a completely automated surface tension meter (KRÜSS-Tensíío type) according to the hanging drop method. The prepared solutions to be tested with different concentration gradients were allowed to stand for at least 24 h before the test and then measured after a constant temperature of 20 min was achieved at 25 °C [41].

3.6. Dynamic Surface Tension (DST)

A DSA25B tensiometer (Krüss Company, Hamburg, Germany) was used at 25.0 ± 0.1 °C to record dynamic surface tension (DST) data. The effective surface ages were within the range of 10 ms to 200 s, with an accuracy of ±0.01 mN/m.

3.7. Cryogenic Transmission Electron Microscopy (Cryo-TEM)

First, an aliquot of 3.5 μL solution (3.0 mg/mL or 1.0 mg/mL) was applied to glow-discharged Quantifiol R 2/1 holey carbon grids and blotted for 3 s under a humidity of 100% at 4 °C before being plunged into liquid ethane using a Vitrobot Mark IV (Thermo

Fisher Scientific, Waltham, MA, USA). The sample structure was immobilized in ice in a glassy state, and then, the sample attached to the copper mesh was transferred to a cryogenic transfer sample rod, followed by TEM imaging to observe the morphology of the 5 g/L solution of C_nDDLPB during a stationary 2-week period [42].

3.8. Dynamic Light Scattering (DLS)

Reverse osmosis (RO) water was used to prepare 5 g/L of C_nDDLPB (n = 8, 10, 12, 14, and 16) samples for measurement. The configured solution needed to be stable and homogeneous, and the temperature was set to 25 °C. An appropriate cuvette was selected, the angle of incident light and other parameters of the instrument were set, the solution (height of 1–1.5 cm) to be measured was added into the cuvette, and it was placed into the sample tank to start the measurement [43,44].

3.9. Wettability Study

According to the seated-drop method, the C_nDDLPB solutions of various concentrations were aspirated using a micro-syringe at 25 °C and dropped onto a polytetrafluoroethylene (PTFE) film. The contact angle was measured using a contact angle meter, and photographs were taken, and the contact angle was recorded at 10 s intervals [45].

3.10. Emulsifying Performance

Emulsification performance analysis testing is commonly conducted using the cylinder method. In a 500 mL iodine flask, 40 mL of the test solution (1.0 g/L) and an equal volume of edible soybean oil are added. The mixture is vigorously shaken up and down five times, followed by a 1 min static period. This process is repeated five times. After completing the aforementioned steps, the mixture is quickly transferred to a 100 mL graduated cylinder, and timing begins immediately. The timing stops when 10 mL of water appears in the lower layer. The time taken for this process is recorded. This experiment is repeated five times to obtain the average value [46].

3.11. Foam Morphology Characterization

According to the Ross–Miles method, the foam performance of C_nDDLPB was evaluated. The prepared solution (1 g/L) was placed in a constant-temperature water bath at (30 ± 0.5) °C for preheating for 30 min. Subsequently, the prepared solution was measured using a foam analyzer. The foam stability was determined based on the initial foam height and the subsequent change in foam height over a specified duration [47].

3.12. Antistatic Performance

The antistatic performance can be tested and analyzed according to GB/T 16801-2013. First, it is necessary to take the fabric finishing agent test solution to pre-treat the polyester fabric samples. Before and after the fabric samples are pre-treated, the surface resistivity is measured using a high resistance meter. The antistatic performance of the fabric finishing agent is evaluated based on the change in surface resistivity or its logarithmic value.

3.13. Salt-Resistant Performance

Prepare a 0.5 g/L solution of the surfactant. Transfer 10 mL of the solution into a test tube, followed by the addition of varying amounts of salt to create solutions of different concentrations. Allow the solutions to stand for 24 h. Subsequently, measure the transmittance of the solutions at 700 nm using a UV-Vis spectrophotometer [48].

3.14. Antibacterial Performance

Prepare a 35% drug stock solution using sterile water and sterilize it by filtration for subsequent use. Streak the tested *Staphylococcus aureus* and *Escherichia coli* on TSA plates and incubate them overnight at 37 °C until visible colonies appear. Select an appropriate quantity of colonies and transfer them to 5 mL of TSB liquid medium for incubation

at a constant temperature of 37 °C for approximately 7 h, or until reaching an OD600 of approximately 0.6. Once the OD600 reaches 0.6 after adjustment with physiological saline, transfer the culture at a 0.1% ratio to TSB solution and incubate it at 37 °C for 18 h. Following incubation, dilute the treated bacterial suspension with PBS, and apply 100 μL of the diluted suspension onto TSA plates. Incubate the plates at 37 °C for 16 h, then photograph and count the colonies for quantification. Select an appropriate dilution gradient from each group for calculating the antibacterial rate.

4. Conclusions

In this study, double-chain lactobionic amide quaternary ammonium salts were synthesized by the amidation of lactobionic acid with N-N-dimethyldipropyltriamine to obtain glycosylamides, followed by quaternization with bromoalkanes of different chain lengths. The raw materials, intermediates, and target products were analyzed by Fourier transform infrared (FTIR) spectroscopy, proton nuclear magnetic resonance (^{1}H NMR) spectroscopy, (^{13}C NMR) spectroscopy, and electrospray ionization mass spectrometry (ESI-MS). The results indicated the successful synthesis of the target product. Through measurements including equilibrium surface tension, dynamic light scattering, and transmission electron microscopy, the surface activity, adsorption, and aggregation behavior of these compounds in aqueous solutions were investigated. Additionally, their application properties such as wetting ability, emulsification capability, foamability, antistatic performance, salt tolerance, and antibacterial activity were analyzed.

The CMC values of the five double-chain lactose amide quaternary ammonium salts (C_nDDLPB) decreased in the order of C_8DDLPB > C_{10}DDLPB > C_{12}DDLPB > C_{14}DDLPB > C_{16}DDLPB. With the growth of the carbon chain, the CMC of the lactose amide quaternary ammonium salts (C_nDDLPB) decreased, and the products exhibited a good surface activity, which can reduce the surface tension of water to 27.82 mN/m. The solutions of compounds with carbon chain lengths ranging from 8 to 14 demonstrate favorable wetting and spreading properties on PTFE, with contact angles decreasing to 33°~40°.TEM images revealed that, except for C_8DDLPB, the other products could form stable vesicle systems in an aqueous solution.

In terms of applications, C_{14}DDLPB exhibits the best emulsification performance on soybean oil, with a time of 16.6 min. The foaming properties of C_nDDLPB are generally low, characteristic of typical low-foaming products. Both C_8DDLPB and C_{10}DDLPB demonstrate excellent antistatic properties, comparable to the commonly used antistatic agent SN. C_8DDLPB and C_{14}DDLPB show good salt tolerance to NaCl, $CaCl_2$, and $MgSO_4$, with light transmittance exceeding 85% at a salt concentration of 50 g/L. Particularly, C_{12}DDLPB displays excellent antibacterial activity against *Escherichia coli* and *Staphylococcus aureus*, with inhibition rates reaching 99.29% and 95.28%, respectively, at a concentration of 350 ppm.

Therefore, this product is a novel glucosamine-based cationic surfactant characterized by low foaming, antibacterial properties, antistatic properties, salt resistance, and the ability to form stable vesicular systems. It holds promise pertaining to applications in various fields such as drug delivery carriers, biomimetic membranes, microreactors, daily chemical industry, and food industry in the future.

Supplementary Materials: The following Supporting Information can be downloaded at: https://www.mdpi.com/article/10.3390/molecules29122749/s1, Figure S1: FT-IR spectra of (a) N-N-Dimethyldipropyltriamine, (b) Lactobionic Acid, (c) DDLPD; Figure S2: ^{1}H-NMR spectra of DDLPD; Figure S3: ^{1}H-NMR spectra of C_8DDLPB ; Figure S4: ^{1}H-NMR spectra of C_{10}DDLPB ; Figure S5: ^{1}H-NMR spectra of C_{12}DDLPB ; Figure S6: ^{1}H-NMR spectra of C_{14}DDLPB ; Figure S7: ^{1}H-NMR spectra of C_{16}DDLPB; Figure S8: ^{13}C-NMR spectra of DDLPD ; Figure S9: ^{13}C-NMR spectra of C_8DDLPB ; Figure S10: ^{13}C-NMR spectra of C_{10}DDLPB ; Figure S11: ^{13}C-NMR spectra of C_{12}DDLPB ; Figure S12: ^{13}C-NMR spectra of C_{14}DDLPB ; Figure S13: ^{13}C-NMR spectra of C_{16}DDLPB ; Figure S14: ESI-MS spectra of C_8DDLPB ; Figure S15: ESI-MS spectra of C_{10}DDLPB ; Figure S16: ESI-MS spectra of C_{12}DDLPB ; Figure S17: ESI-MS spectra of C_{14}DDLPB; Figure S18: ESI-MS spectra of C_{16}DDLPB; Figure S19: cryo-EM spectra of C_nDDLPB.

Author Contributions: Conceptualization, G.W. and Y.W. (Yan Wang); methodology, L.Z.; software, Z.C.; validation, X.L. (Xiaoming Li); formal analysis, X.L. (Xudong Liu); investigation, Y.W. (Yunkai Wang); resources, E.Z.; data curation, Y.H.; writing—original draft preparation, Y.W. (Yunkai Wang); writing—review and editing, Y.W. (Yunkai Wang); visualization, L.Z.; supervision, M.D.S.; project administration, Z.C.; funding acquisition, L.Z. All authors have read and agreed to the published version of the manuscript.

Funding: This project was funded by the the Taiyuan University of Science and Technology Scientific Initial Funding (No. 20222010), Taiyuan University of Science and Technology Graduate Education Innovation Programme (No. SY2023023), The Nation Natural Science Foundation of China (No. 22178240) for the financial support.

Institutional Review Board Statement: Not applicable.

Informed Consent Statement: Not applicable.

Data Availability Statement: Data are contained within the article and Supplementary Materials.

Conflicts of Interest: Author Ying Huang was employed by the company Taiyuan Hengdeyuan Animal Protection Technology Development and Shanxi Livestock and Poultry Breeding. The remaining authors declare that the research was conducted in the absence of any commercial or financial relationships that could be construed as a potential conflict of interest.

References

1. Du, Q.; Li, Z.; Du, M.; Yang, T. Tianle. Government venture capital and innovation performance in alternative energy production: The moderating role of environmental regulation and capital market activity. *Energy Econ.* **2024**, *129*, 107196. [CrossRef]
2. Yang, T.; Fang, S.; Du, A.; Du, Q. Navigating the nexus: Geopolitical risk, fossil energy prices, and European utility stock returns—Implications for environmental management and energy security in a conflict-ridden global landscape. *J. Environ. Manag.* **2024**, *352*, 120086.
3. Yang, T.; Dong, Q.; Du, Q.; Du, Q.; Du, M. Carbon dioxide emissions and Chinese OFDI: From the perspective of carbon neutrality targets and environmental management of home country. *J. Environ. Manag.* **2021**, *295*, 113120. [CrossRef] [PubMed]
4. Tong, S.; Hu, Y.; Yu, J. Research Progress on Bio-based Vitrimer Materials. *Biomass Chem. Eng.* **2023**, *57*, 37–46.
5. Xue, X.; Wang, S.; Yang, T.; He, M.; Tang, X. Preparation and photocatalytic performance of Cu/cellulose-based TiO_2 composite. *New Chem. Mater.* **2022**, *50*, 195–200.
6. Gericke, M.; Amaral, A.J.R.; Budtova, T.; Tatiana, B.; Pieter, D.; Thomas, G.; Thomas, H.; Herman, H.; Anton, H.; Olli, I.; et al. The European Polysaccharide Network of Excellence (EPNOE) research roadmap 2040: Advanced strategies for exploiting the vast potential of polysaccharides as renewable bioresources. *Carbohydr. Polym.* **2024**, *326*, 121633. [CrossRef] [PubMed]
7. Martínez, A.; Magallanes, L.; Tarditto, L.; María C, P.; María F, G. María. Fatty acids methyl esters from soybean oil for biobased surfactants industry: Obtention C16 C18 concentrate for use as feedstock. *Ind. Crops Prod.* **2022**, *190*, 115892. [CrossRef]
8. Reid, A.G.; Eswara Rao, C.A.; Abhay, A.; Taylor, U.; Ravikumar R, G.; Avantika, S.; Jason S, D.; Gregg T, B.; Eugene, C. Bio-based lactone acrylic plastics with performance and recyclability advantages. *Cell Rep. Phys. Sci.* **2024**, *5*, 101938.
9. Thuy, T.H.N.; Wahyu, S.P.; Jun-Chul, C.; Norihisa, F.; Satoshi, T.; Takehiro, Y.; Nobuo, H.; Sho, K. Design and Evaluation of Bio-Based Industrial Symbiosis System Producing Energy and Chemicals Using Regionally Available Crop Residue. *Resour. Conserv. Recycl.* **2024**, *204*, 107509.
10. Lu, H.; Pezron, I.; Gaudin, T.; Audrey, D. Non-equilibrium micelles formed by sugar-based surfactants under their Krafft temperature. *Colloids Surf. A Physicochem. Eng. Asp.* **2018**, *540*, 167–176. [CrossRef]
11. Syguda, A.; Ławniczak, Ł.; Wróbel, P.; Filip, W.; Grzegorz, F.; Anna, P.; Marta, W.; Michał, N.; Aleksandra, G.; Łukasz, C. Biodegradable amidequats, derivatives of caprylic and pelargonic acids as cationic surfactants for agricultural applications. *J. Mol. Liq.* **2023**, *391*, 123221. [CrossRef]
12. Siddiqui, U.; Aslam, J.; Ansari, W.; Din, K. Micellization and aggregation behavior of a series of cationic gemini surfactants (m-s-m type) on their interaction with a biodegradable sugar-based surfactant (octyl-β-D-glucopyranoside). *Colloids Surf. A Physicochem. Eng. Asp.* **2013**, *421*, 164–172. [CrossRef]
13. Lee, S.; Lee, J.; Yu, H.; JongChoo, L. Synthesis of environment friendly nonionic surfactants from sugar base and characterization of interfacial properties for detergent application. *J. Ind. Eng. Chem.* **2016**, *38*, 157–166. [CrossRef]
14. Guido, V.; Pierluigi, Q.; Claudia, B.; Savarino, P.; Barni, E.; Fisicaro, E. Synthesis and Surface and Antimicrobial Properties of Novel Cationic Surfactants. *J. Org. Chem.* **2000**, *65*, 8197–8203.
15. Wojciech, S.; Natalia, B.; Michal, H. Evaluation of surface active and antimicrobial properties of alkyl D-lyxosides and alkyl L-rhamnosides as green surfactants. *Chemosphere* **2021**, *271*, 129818.
16. Zhi, L.; Zhang, E.; Shi, X. Research progress of glycosyl cationic surfactants. *Huaxue Tongbao* **2022**, *85*, 790–801.

17. Lu, B.; Vayssade, M.; Miao, Y.; Vincen, C.; Eric, G.; Anne, W.; Denis, P.; Audrey, D.; Christophe, E.; Isabelle, P. Physico-chemical properties and cytotoxic effects of sugar-based surfactants: Impact of structural variations. *Colloids Surf. B Biointerfaces* **2016**, *145*, 79–86. [CrossRef] [PubMed]
18. Cheng, W.; Yu, L.; Cheng, G. Synthesis characterization and application of Bola silicone quaternary ammonium salt. *CIESC J.* **2021**, *72*, 2837–2848.
19. Vargas-Ruiz, S.; Soltwedel, O.; Micciulla, S. Sugar Surfactant Based Microemulsions at Solid Surfaces: Influence of the Oil Type and Surface Polarity. *Langmuir ACS J. Surf. Colloids* **2016**, *32*, 11928–11938. [CrossRef]
20. Salomé, V.; Jana, L.; Regine, V.; Thomas, H.; Stefan, W. Wetting of planar solid surfaces by bicontinuous sugar surfactant-based microemulsions. *Colloid Polym. Sci.* **2017**, *295*, 2183–2190.
21. Wang, X.; Hao, J. Ionogels of Sugar Surfactant in Ethylammonium Nitrate: Phase Transition from Closely Packed Bilayers to Right-Handed Twisted Ribbons. *J. Phys. Chem. B* **2015**, *119*, 13321–13329. [CrossRef] [PubMed]
22. Wen, P.; Sun, Y.; Sun, J. Properties of ethoxylated tris-ester-based quaternary ammonium salts. *Deterg. Cosmet.* **2014**, *37*, 69–71.
23. Dufour, A.; Thiébaut, D.; Ligiero, L.; Matthieu, L.; Vial, J. Chromatographic behavior and characterization of polydisperse surfactants using Ultra-High-Performance Liquid Chromatography hyphenated to High-Resolution Mass Spectrometry. *J. Chromatogr. A* **2020**, *1614*, 460731. [CrossRef] [PubMed]
24. Rosen, M.J.; Kunjappu, J.T. *Surfactants and Interfacial Phenomena*, 4th ed.; Wiley: Hoboken, NJ, USA, 2012; pp. 336–367.
25. Fainerman, V.B.; Miller, R.; Aksenenko, E.V.; Makievski, A.V. 3. Equilibrium adsorption properties of single and mixed surfactant solutions. *Stud. Interface Sci.* **2001**, *13*, 189–285.
26. Wang, T.; Xu, P.; Ma, A. Effect of hydrophobic chain length on surface activity of gemini betaine. *Chem. Res. Appl.* **2021**, *33*, 2210–2216.
27. Aratono, M.; Onimaru, N.; Yoshikai, Y.; Makiko, S.; Ikuyo, K.; Kanda, W.; Akio, O.; Takanori, T.; Belkoura, L.; Reinhard, S.; et al. Spontaneous vesicle formation of single chain and double chain cationic surfactant mixtures. *J. Phys. Chem. B* **2007**, *111*, 107–115. [CrossRef]
28. Johnsson, M.; Wagenaar, A.; Engberts, J.B. Sugar-based gemini surfactant with a vesicle-to-micelle transition at acidic pH and a reversible vesicle flocculation near neutral pH. *J. Am. Chem. Soc.* **2003**, *125*, 757–760. [CrossRef]
29. Yun, Y.; Xiong, W.; Li, X.; Lu, T.; Huang, G.; Li, Z.; Fu, H. Molecular Packing Parameter in Bolaamphiphile Solutions: Adjustment of Aggregate Morphology by Modifying the Solution Conditions. *J. Phys. Chem. B* **2007**, *111*, 2225–2230. [CrossRef]
30. Gong, J.; Song, Y.; Sun, Y.; Sun, Q.; Liu, C.; Tan, J.; Zhao, L.; Xu, B. Vesicle-to-micelle transition in a double chain quaternary ammonium surfactant system: Interfacial behavior and molecular insights. *J. Mol. Liq.* **2024**, *394*, 123714. [CrossRef]
31. Xia, Y.; Goldmints, I.; Johnson, P.; Alan, T.; Arijit, B. Temporal Evolution of Microstructures in Aqueous CTAB/SOS and CTAB/HDBS Solutions. *Langmuir ACS J. Surf. Colloids* **2002**, *18*, 3822–3828. [CrossRef]
32. Hsieh, A.; Franses, E.; Corti, D. Formation of gem-like dispersions of soft crystallites in water by vesicles of a cationic surfactant. *Colloids Surf. A Physicochem. Eng. Asp.* **2022**, *652*, 129822. [CrossRef]
33. Surajit, G.; Chiranjib, G.; Chiranjib, B.; Sarthak, M.; Jagannath, K.; Nilmoni, S. Spontaneous Transition of Micelle–Vesicle–Micelle in a Mixture of Cationic Surfactant and Anionic Surfactant-like Ionic Liquid: A Pure Nonlipid Small Unilamellar Vesicular Template Used for Solvent and Rotational Relaxation Study. *Langmuir ACS J. Surf. Colloids* **2013**, *29*, 10066–10076.
34. Akihisa, S.; Alan, H. Model for Formation and Growth of Vesicles in Mixed Anionic/Cationic (SOS/CTAB) Surfactant Systems. *Langmuir ACS J. Surf. Colloids* **2002**, *18*, 7341–7348.
35. Zhang, B.; Yao, X.; Li, P.; Guo, C.; Ren, X.; Li, J. Preparation of chitosan sulfate and vesicle formation with a conventional cationic surfactant. *Carbohydr. Polym.* **2018**, *183*, 240–245. [CrossRef] [PubMed]
36. Li, Z.; Zhao, K.; Wang, Y.; Zheng, Z.; Zhang, C.; Gao, Y.; Du, F. Droplet splash and spread on superhydrophobic lotus leaves: Direct regulation by tuning the chain length of surfactant. *Colloids Surf. A Physicochem. Eng. Asp.* **2022**, *648*, 129178. [CrossRef]
37. Katarzyna, M.; Katarzyna, S.; Daniela, G.; Daria, W. Synthesis, Surface and Antimicrobial Activity of New Lactose-Based Surfactants. *Molecules* **2019**, *24*, 4010.
38. Zhi, L. *Synthesis and Properties of Novel Gluconamide-Type Surfactants*; ShanXi University: Taiyuan, China, 2014.
39. Jiang, J.; Zou, Y.; Sun, Q. Copolymers functionalized with quaternary ammonium compounds under template chain exhibit simultaneously efficient bactericidal and flocculation properties: Characterization, performance and mechanism. *J. Hazard. Mater.* **2024**, *465*, 133476. [CrossRef] [PubMed]
40. Wang, J.; Yang, X.; Chen, Y.; Zou, W. Bactericidal activity of sugar-based cationic gemini surfactants. *China Surfactant Deterg. Cosmet.* **2019**, *49*, 83–86.
41. Dou, J.; Liu, J.; Wang, G. Surface Activity, Wetting, and Aggregation of a Perfluoropolyether Quaternary Ammonium Salt Surfactant with a Hydroxyethyl Group. *Molecules* **2023**, *28*, 7151. [CrossRef]
42. Ram-On, M.; Cohen, Y.; Talmon, Y. Effect of Polyelectrolyte Stiffness and Solution pH on the Nanostructure of Complexes Formed by Cationic Amphiphiles and Negatively Charged Polyelectrolytes. *J. Phys. Chem. B* **2016**, *120*, 5907–5915. [CrossRef]
43. Matthew, L.L.; Tom, K.; Michael, R.W. Anticipating colloidal instabilities in cationic vesicle dispersions by measuring collective motions with dynamic light scattering. *J. Colloid Interface Sci.* **2006**, *296*, 599–607.
44. Milad, E.; Karin, S.; Stoyan, I.; Nikolay, G.; Kerstin, E. Oppositely charged surfactants and nanoparticles at the air-water interface: Influence of surfactant to nanoparticle ratio. *J. Colloid Interface Sci.* **2024**, *653*, 1388–1401.

45. Shi, X.; Zeng, M.; Xu, X.; Liu, Y.; Kou, J.; Bian, Q.; Song, H.; Zhang, J.; Wang, Q. Promotion of droplet deposition, diffusion-wetting and retention on hydrophobic surfaces by nonionic star-shaped oligomeric surfactants. *J. Mol. Liq.* **2023**, *386*, 122521. [CrossRef]
46. Cao, Y.; Yang, W.; Jiang, Y. Synthesis and properties of a zwitterionic Gemini surfactant. *Fine Chem.* **2021**, *38*, 335–340.
47. Ning, B.; Zhang, M.; Bai, Y.; Wang, W.; Wang, G. Comparison of the properties of perfluoroalkyl polyoxyethylene ether and alkyl polyoxyethylene ether. *Colloid Polym. Sci.* **2020**, *298*, 1389–1399. [CrossRef]
48. Hu, Y.; Xu, Z.; Li, Y. Synthesis and application performance of branched chain alcohol ether sodium sulfate based on SO3 sulfonation. *Text. Aux.* **2022**, *39*, 37–40.

Disclaimer/Publisher's Note: The statements, opinions and data contained in all publications are solely those of the individual author(s) and contributor(s) and not of MDPI and/or the editor(s). MDPI and/or the editor(s) disclaim responsibility for any injury to people or property resulting from any ideas, methods, instructions or products referred to in the content.